Improved Fluorescence Excitation-Emission Matrix Regional Integration to Quantify Spectra for Fluorescent Dissolved Organic Matter

Jie Zhou, Jun-Jian Wang, Antoine Baudon, and Alex T. Chow*

The purpose of this short communication is to demonstrate the importance of numerical analysis and wavelength increment selection when characterizing fluorescent dissolved organic matter (FDOM) using fluorescence excitation–emission matrix (EEM) regional integration. A variety of water samples, representing a landscape gradient and different types of FDOM, were analyzed for their percentage distribution of five operationally defined FDOM fractions (aromatic protein I, aromatic protein II, fulvic acid–like, soluble microbial byproduct–like, and humic acid–like) using three numerical methods in integrating volume under the surface of the fluorescence EEMs: Riemann summation, composite trapezoidal rule, and composite Simpson's rule. The influence of wavelength increment was also examined for the precision of the percentage distribution of each fraction. Our results show that the FDOM fraction estimated by Riemann summation with a 10- or 5-nm excitation wavelength can cause >40% or >5% errors, respectively, when compared with the best estimated values obtained by averaging results from composite trapezoidal rule and composite Simpson's rule with 1-nm excitation wavelength at the same emission increment. Also, our experiments show that fluorescence matrix regional integration could underestimate the two aromatic protein fractions but could overestimate the soluble microbial byproduct–like and humic acid–like fractions if improper increment and integral methods are used. The error can be reduced if a smaller wavelength increment is used. The smallest increment in a spectrofluorometer and composite Simpson's rule should be used for scanning fluorescence EEMs and calculating the percentage distribution of each FDOM fraction. Alternatively, 5-nm wavelength increments with composite Simpson's rule could be cost effective, and the error of each FDOM fraction commonly falls within 5% compared with those estimated by 1-nm increments.

J. Environ. Qual. 42:925–930 (2013)
doi:10.2134/jeq2012.0460
Supplemental data file is available online for this article.
Received 3 Dec. 2012.
*Corresponding author (achow@clemson.edu).

Excitation–emission matrix (EEM) fluorescence spectroscopy has been widely used to characterize and monitor fluorescent dissolved organic matter (FDOM) in marine, freshwater, soil, and wastewater samples. This technique has the advantages of being nondestructive, highly sensitive, rapid, and relatively inexpensive (Hudson et al., 2007; Henderson et al., 2009; Fellman et al., 2010). Filtered water samples are typically irradiated with excitation wavelengths from 240 to 450 nm and emission wavelengths recorded from 250 to 600 nm. Depending on the increments of the wavelengths set in the instruments, an EEM could contain hundreds to over 10,000 wavelength-dependent fluorescence intensity data points. Interpreting this data set has posed a significant challenge. Visual inspection of fluorescence peaks with comparison of the intensity of individual peaks is a common technique for analyzing EEMs (Coble, 1996; Hudson et al., 2007). Recently, various mathematical techniques have been used to interpret the wavelength-dependent fluorescence intensity data points represented in EEMs. Parallel factor analysis (PARAFAC) and fluorescence regional integration (FRI) are two commonly used methods. Parallel factor analysis is a multivariate modeling technique that decomposes the fluorescence signature of FDOM into individual components and provides estimates of the relative contribution of each component of total FDOM fluorescence (Stedmon et al., 2003; Fellman et al., 2010). Fluorescence regional integration is a quantitative technique that integrates the volumes beneath operationally defined EEM regions, and the normalized region-specific EEM volumes represent the relative abundance of FDOM fractions in a water sample (Chen et al., 2003). The advantage of the FRI technique is to analyze FDOM through quantitative use of all the wavelength-dependent fluorescence intensity data from EEMs. It has the ability to capture the heterogeneity of FDOM. In addition, FRI could provide information about the composition (i.e., relative abundance of operationally defined fractions) of FDOM in a relatively short time, comparing with other fractionation techniques that require days to perform (Chow et al., 2005). Fluorescence regional integration has been widely used for many environmental settings to characterize FDOM, including landfill leachates, bioreactors,

J. Zhou and A. Baudon, Dep. of Mathematics and Statistics, Coastal Carolina Univ., Conway, SC 29528; J.-J. Wang and A.T. Chow, Baruch Institute of Coastal Ecology & Forest Science, Clemson Univ., Georgetown, SC 29440. Assigned to Associate Editor Tsutomu Ohno.

Abbreviations: EEM, excitation–emission matrix; FDOM, fluorescent dissolved organic matter; FRI, fluorescence region integration; PARAFAC, parallel factor analysis.

and drinking water (Wang et al., 2009; Massicotte and Frenette, 2011; He et al., 2011; Wu et al., 2012). The PARAFAC and FRI techniques involve mathematical manipulation on the discrete data in EEMs. In this paper, we address the issues of numerical analysis on the FRI and examine the effects of different integration methods on the precision of EEM analyses.

In the original paper by Chen et al. (2003), five regions in an EEM were operationally defined using consistent excitation (ex) and emission (em) wavelength boundaries based on fluorescence of model compounds and FDOM fractions: Region I, aromatic protein I (ex: 200–250 nm; em: 280–330 nm); Region II, aromatic protein II (ex: 200–250 nm; em: 330–380 nm); Region III, fulvic acid–like (ex: 200–250 nm; em: 380–550 nm); Region IV, soluble microbial byproduct–like (250 nm < ex < 400 nm; em: 280–380 nm); and Region V, humic acid–like (250 nm < ex < 400 nm; em: 380–550 nm). The areas of the five defined regions are not the same. Region V has the largest area, and Region I has the smallest area. The total volume (ϕ_v) beneath Region V could be always greater than the volume (ϕ_1) in Region I. To account the area effect, the intensity per unit area [(sum of the intensity/(excitation wavelength × emission wavelength)] should be calculated. Volumetric integration under the EEM within each region is normalized to the projected excitation–emission area within that region and dissolved organic carbon concentration. It results in a normalized region-specific EEM volume (Chen et al., 2003).

The volume (ϕ_i) beneath region *i* of an EEM can be calculated using Eq. [1]:

$$\phi_i = \int_{ex}\int_{em} I(\lambda_{ex}\lambda_{em})d\lambda_{ex}d\lambda_{em} \quad [1]$$

where $d\lambda_{ex}$ is the differential of the excitation wavelength, $d\lambda_{em}$ is the differential of the emission wavelength, and $I(\lambda_{ex}\lambda_{em})$ is the fluorescence intensity at each excitation–emission wavelength pair. For discrete data, Riemann summation is used to quantify the volume of each region, as shown in Eq. [2]:

$$\phi_i = \sum_{ex}\sum_{em} I(\lambda_{ex}\lambda_{em})\Delta\lambda_{ex}\Delta\lambda_{em} \quad [2]$$

where $\Delta\lambda_{ex}$ and $\Delta\lambda_{em}$ are the excitation and emission wavelength increments, respectively. In this integration method, the volume of a rectangular box under a particular point is calculated, and the volume of the region *i* is the sum of these rectangular boxes within the region. However, this commonly used numerical analysis could underestimate the volume if the surface is monotonically increased or overestimate the volume if the surface is monotonically decreased (Burden and Faires, 2001). Ideally, the error in the integration is zero if the intervals are infinitesimally small, but spectrofluorometers can provide only discrete data. The precision can be improved by using smaller excitation and emission increments, but such an approach will extend the experimental time and shorten the lifetime of the xenon lamp in a spectrofluorometer.

The objective of this study was to compare different numerical methods and increments of excitation wavelengths on the precision of determining the volume beneath each defined region of an EEM and the normalized percentages of different FDOM fractions, which are used to quantify the chemical properties of FDOM. Specifically, the composite trapezoidal rule and the composite Simpson's rule were examined, and results were compared with that of the more commonly used method—the Riemann summation.

Materials and Methods

Fluorescent Dissolved Organic Matter

A variety of water samples representing landscape gradient and different types of FDOM (summarized in Supplemental Table S1) were used to test the numerical methods for volume calculation under the EEM surface. Samples were selected so that visible peaks were observed in the five operationally defined regions. Four ecosystems representing a salinity gradient from freshwater to marine water along an approximately 3-km transect on Hobcaw Barony in Georgetown, South Carolina were sampled in January 2012, including a cypress-tupelo-pine forest on Crabhaul Road, a forested wetland at Reserve Bank Road North, a brackish water wetland at Reserve Bank Road, and a salt marsh at Thousand Acre Field. Two river water samples were collected in the same month from urban and agricultural watersheds of Huckleberry Branch and Black Creek within the Pee Dee basin near Quinby, South Carolina. All water samples collected in the field were stored on ice immediately and transferred to the laboratory for processing within the same day. Leaf litter of baldcypress (*Taxodium distichum*), longleaf pine (*Pinus palustris*), and water tupelo (*Nyssa aquatica*) were collected with nets from an undisturbed forested wetland on Hobcaw Barony in fall 2011. Litter samples were oven dried at 50°C overnight, ground, and passed through a 0.5-mm sieve. One gram of dried material was mixed with 50 mL Milli-Q water and shaken at room temperature for 8 h. All water samples and litter extracts were filtered through a 0.45-μm polyethersulfone membrane (Supor-450, Pall Corp.). All filters were prewashed with at least 100 mL Milli-Q water before sample filtration. Some chemical properties of the water samples and litter extracts are summarized in Supplemental Table S1.

Fluorescence Measurement

Fluorescence scans in this study were done in a Shimadzu spectrofluorometer RF5301 with a 5-nm slit in excitation and a 5-nm slit in emission. Scans were first corrected against a water blank to remove most of the first- and second-order Raman scattering. Scans were standardized to Raman's units (normalized to the integral of the Raman signal between 390 and 410 nm in emission at a fixed excitation of 350 nm) with a Milli-Q water sample run the same day as the samples as suggested in Lawaetz and Stedmon (2009). To account for reabsorption of the light emitted by fluorophores in a concentrated water sample, all samples were diluted with Milli-Q water to an ultraviolet absorbance at 254 nm of 0.3 or less (Miller et al., 2010). The UV scan was conducted in Shimadzu UV-1800 UV-VIS spectrophotometer. Fluorescence EEM and UV measurements used quartz cuvettes with 1-cm paths for analyses. Fluorescence spectra for all water samples were scanned in S mode (i.e., monitoring only the signal from the sample), with excitation from 220 to 450 nm and emission from 220 to 550 nm with a respond time of 0.25 s and scan speed set at "Very Fast." The EEMs were corrected for instrument biases using an excitation correction spectrum derived from a concentrated solution of rhodamine B and an emission correction spectrum

obtained using a ground-quartz diffuser as recommended by the manufacturer (Cory et al., 2010). The remaining first-order Rayleigh scattering was removed by the insertion of missing values (not a number) in a ±10-nm diagonal band where excitation is equal to the emission wavelength. Because the increment interval for emission was set constant at 1 nm, three intervals for excitation were compared at 10 nm (EX10), 5 nm (EX5), and 1 nm (EX1) for each sample measurement, and the corresponding measuring times were recorded. A 5-nm excitation step is commonly used in water research.

Fluorescence Regional Integration

The lowest emission and excitation wavelength in the Shimadzu RF5301 is 220 nm. Therefore, the five regions in EEMs in this study were defined as follows: Region I, aromatic protein I (ex: 220–250 nm; em: 280–330 nm); Region II, aromatic protein II (ex: 220–250 nm; em: 330–380 nm); Region III, fulvic acid–like (ex: 220–250 nm; em: 380–550 nm); Region IV, soluble microbial byproduct–like (250 nm < ex < 450 nm; em: 280–380 nm); and Region V, humic acid–like (250 nm < ex < 450 nm; em: 380–550 nm). The normalized excitation–emission area volumes ($\Phi_{i,n}$) and normalized percentage ($P_{i,n}$) were calculated according to Chen et al. (2003) using Eq. [3]:

$$\Phi_{i,n} = MF_i \Phi_i$$
$$P_{i,n} = \Phi_{i,n} / \sum_{i=1}^{5} \Phi_{i,n} \quad [3]$$

where the MF_i is a multiplication factor for each region, equal to the inverse of the fractional projected excitation–emission area.

Volumes under each EEM were calculated using three numerical methods in this study: (i) the Riemann summation, (ii) the composite trapezoidal rule, and (iii) the composite Simpson's rule. When using the trapezoidal rule, rectangles used in the Riemann summation are replaced with trapezoids. With Simpson's rule, a strip under a parabolic curve that passes through three adjacent points is used. To find the volume of a two-variable function, we need to apply the methods on each dimension. Assuming the range of the emission wavelength is from a to b and the range of the excitation wavelength is from c to d, let λ_{emk} be the emission wavelength point on $[a, b]$, $\lambda_{emk} - \lambda_{emk-1} = \Delta\lambda_{em}$ for $k = 1, 2,..., n$, where $\lambda_{em0} = a$ and $\lambda_{emn} = b$; λ_{exl} is the excitation wavelength point on $[c, d]$, $\lambda_{exl} - \lambda_{exl-1} = \Delta\lambda_{ex}$ for $l = 1, 2,..., m$, where $\lambda_{ex0} = c$, $\lambda_{exm} = d$. $I(\lambda_{exl}\lambda_{emk})$ is the fluorescence intensity at the excitation–emission wavelength pair (λ_{exl}, λ_{emk}). The Riemann summation is used to quantify the volume of each region (see Eq. [2]).

The formula for the composite trapezoidal rule is shown in Eq. [4]:

$$\begin{aligned}\phi_i = \frac{\Delta\lambda_{ex}\Delta\lambda_{em}}{4}[&I(\lambda_{ex0}\lambda_{em0}) + I(\lambda_{exm}\lambda_{em0}) + I(\lambda_{ex0}\lambda_{emn}) \\ &+ I(\lambda_{exm}\lambda_{emn}) + 2\sum_{l=1}^{m-1} I(\lambda_{exl}\lambda_{em0}) + 2\sum_{l=1}^{m-1} I(\lambda_{exl}\lambda_{emn}) \\ &+ 2\sum_{k=1}^{n-1} I(\lambda_{ex0}\lambda_{emk}) + 2\sum_{k=1}^{n-1} I(\lambda_{exm}\lambda_{emk}) + 4\sum_{k=1}^{n-1}\sum_{l=1}^{m-1} I(\lambda_{exl}\lambda_{emk})]\end{aligned} \quad [4]$$

The formula for composite Simpson's rule is shown in Eq. [5]:

$$\begin{aligned}\phi_i = \frac{\Delta\lambda_{ex}\Delta\lambda_{em}}{9}[&I(\lambda_{ex0}\lambda_{em0}) + I(\lambda_{exm}\lambda_{em0}) \\ &+ I(\lambda_{ex0}\lambda_{emn}) + I(\lambda_{exm}\lambda_{emn}) \\ &+ 2\sum_{l=1}^{\frac{m}{2}-1} I(\lambda_{ex2l}\lambda_{em0}) + 2\sum_{l=1}^{\frac{m}{2}-1} I(\lambda_{ex2l}\lambda_{emn}) \\ &+ 2\sum_{k=1}^{\frac{n}{2}-1} I(\lambda_{ex0}\lambda_{em2k}) + 2\sum_{k=1}^{\frac{n}{2}-1} I(\lambda_{exm}\lambda_{em2k}) \\ &+ 4\sum_{l=1}^{\frac{m}{2}} I(\lambda_{ex2l-1}\lambda_{em0}) + 4\sum_{l=1}^{\frac{m}{2}} I(\lambda_{ex2l-1}\lambda_{emn}) \\ &+ 4\sum_{k=1}^{\frac{n}{2}} I(\lambda_{ex0}\lambda_{em2k-1}) + 4\sum_{k=1}^{\frac{n}{2}} I(\lambda_{exm}\lambda_{em2k-1}) \\ &+ 4\sum_{k=1}^{\frac{n}{2}-1}\sum_{l=1}^{\frac{m}{2}-1} I(\lambda_{ex2l}\lambda_{em2k}) + 8\sum_{k=1}^{\frac{n}{2}-1}\sum_{l=1}^{\frac{m}{2}} I(\lambda_{ex2l-1}\lambda_{em2k}) \\ &+ 4\sum_{k=1}^{\frac{n}{2}}\sum_{l=1}^{\frac{m}{2}-1} I(\lambda_{ex2l}\lambda_{em2k-1}) + 16\sum_{k=1}^{\frac{n}{2}}\sum_{l=1}^{\frac{m}{2}} I(\lambda_{ex2l-1}\lambda_{em2k-1})]\end{aligned} \quad [5]$$

Detailed mathematical expressions of these methods can be found in books about numerical analysis (e.g., Burden and Faires, 2001). The volumes of the five fractions were calculated within the defined boundaries as described above. A MATLAB program was developed based on these three methods to calculate the normalized percentage of each fraction. The codes for the composite trapezoidal rule and the composite Simpson's rule are shown in Supplemental Boxes S1 and S2, respectively. Because the exact function of the EEM surface is not defined, the average volume calculated by the composite trapezoidal rule and composite Simpson's rule at excitation 1 nm is used for our control because, theoretically, the composite trapezoidal rule and the composite Simpson's rule converge to the actual value faster than the Riemann summation under the same setting (Burden and Faires, 2001). Error analysis at other wavelength increments and Riemann summation were compared with this control value.

Error Analysis

The precision of each method is determined by comparing the approximation bounds, and the formula of each method in two-dimensional cases can be diverse. Assuming that the range of the emission wavelength is from a to b and the range of the excitation wavelength is from c to d, the error of the Riemann summation is bounded by

$$\left|\frac{(b-a)(d-c)}{2}[\Delta\lambda_{ex} I'(\eta,\mu) + \Delta\lambda_{em} I'(\hat{\eta},\hat{\mu})]\right|$$

where η, $\hat{\eta}$ are on the interval $[c, d]$; μ, $\hat{\mu}$ are on the interval $[a, b]$; and I' is the first derivative of the function I. The approximation error for the composite trapezoidal rule is bounded by

$$\left|\frac{(d-c)(b-a)}{12}[(\Delta\lambda_{ex})^2 I''(\eta,\mu) + (\Delta\lambda_{em})^2 I''(\hat{\eta},\hat{\mu})]\right|$$

where η, $\hat{\eta}$ are on the interval [c, d]; μ, $\hat{\mu}$ are on the interval [a, b]; and I'' is the second derivative of function I. The error bound for the composite Simpson's rule is

$$\left|\frac{(d-c)(b-a)}{180}[(\Delta\lambda_{ex})^4 I^{(4)}(\eta,\mu)+(\Delta\lambda_{em})^4 I^{(4)}(\hat{\eta},\hat{\mu})]\right|$$

where η, $\hat{\eta}$ are on the interval [c, d]; μ, $\hat{\mu}$ are on the interval [a, b]; and $I^{(4)}$ is the fourth derivative of the function I.

The error of composite Simpson's rule goes to zero faster than the other two methods as $\Delta\lambda_{em}$ and $\Delta\lambda_{ex}$ get smaller. However, it comes with the constraint that the number of data points in each direction (i.e., excitation wavelength direction and emission wavelength direction) has to be odd. In practice, we can combine the composite Simpson's rule and the trapezoidal rule when the number of data points is even. In this case, we recommend applying the trapezoidal rule on the first interval or the last interval and the composite Simpson's rule on the remaining intervals to achieve the better precision.

Results and Discussion

Characteristics of Fluorescent Dissolved Organic Matter

The normalized percentage distributions of the five FDOM fractions of all tested samples calculated using the composite trapezoidal rule and composite Simpson's rule with excitation wavelength at 1-nm increments are basically identical, with less than 0.01% differences in all regions. Their average at excitation 1 nm and emission 1 nm are considered as the best estimation, and the results are summarized in Supplemental Table S2. In general, the fluorescence EEM spectra of our natural water samples had similar regional distribution (FDOM fractions), with high peaks in Regions III and V (Fig. 1d). Our modified FRI method estimated that 44 to 48% and 21 to 27% of FDOM are fulvic acid–like (Region III) and humic acid–like compounds (Region V), respectively. Aromatic protein–like compounds in Region II were also an important fraction in our natural water samples, representing 16 to 20% of FDOM. Soluble microbial byproduct-like compounds in Region IV and aromatic protein–like compounds in Region I were relatively minor, representing less than 10% of FDOM individually (Supplemental Table S2). Unlike natural water samples collected in river, forest, wetland, and estuary ecosystems, the EEMs of litter extracts show significant peaks in Regions I, II, and IV (Fig. 1). For example, baldcypress litter extracts had the greatest fraction of aromatic protein–like compounds in Region II and microbial byproduct-like compounds in Region IV, whereas water tupelo and longleaf pine extracts had dominant fractions of aromatic protein–like compounds in Region I and microbial byproduct–like compounds in Region IV. Aromatic protein–like compounds (Regions I and II) in litter extracts were greater than 55%. Humic acid–like and fulvic acid–like fractions in these samples are relatively minor. In this study, we are only interested in evaluating the effects of numerical analysis on the volume calculation. The volume relationships with chemical properties have been verified in previous publications, and details can be found in Chen et al. (2003).

Integral Methods and Wavelength Increments in Numerical Analysis

The errors in normalized percentage distribution of selected samples measured at three excitation increments and three numerical methods are summarized in Supplemental Tables S3 and S4. Regardless of the integral method, up to 40% error was observed when a 10-nm excitation increment was used. Errors were remarkably reduced and accuracies were enhanced when the excitation increment was decreased to 5 nm. The precision of volume and normalized percentage assessments was much better using 1-nm excitation increments compared with 10- and 5-nm excitation increments. From a 10-nm excitation increment to a 1-nm excitation increment, with more data points being collected, the calculated volumes approached the actual volumes, regardless of integral methods. Noticeably, FDOM fractions in region II are always underestimated, but FDOM fractions in regions IV and V are overestimated when compared with the control no matter what integral methods and or excitation intervals are used. This error is not a random error and is due to the shape of the EEM surface in the region. The FRI technique operationally defines the five regions, and some regions could only contain certain portions of a peak. In

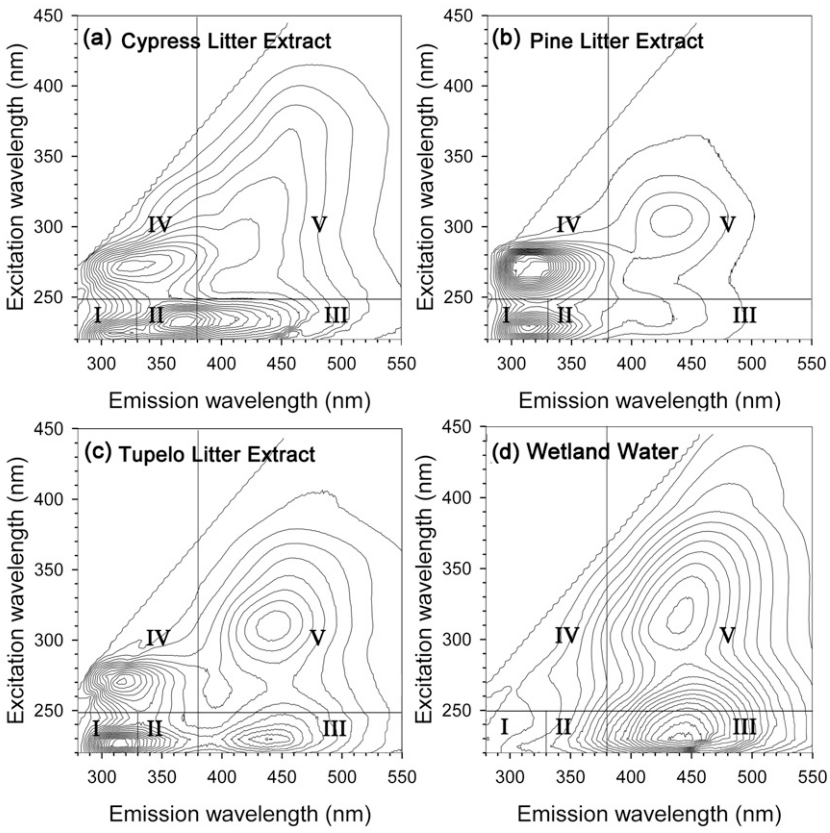

Fig. 1. Fluorescence excitation–emission matrix of three litter extracts and wetland water from Hobcaw Barony. Different from natural water samples, peaks of litter extracts are also found in Regions I, II, and IV.

such cases, numerical analysis could underestimate the volume if the surface is monotonically increased or overestimate the volume if the surface is monotonically decreased (Burden and Faires, 2001).

The estimated integral volume was affected by the integral method we used and by the data-collecting increments (i.e., increments of excitation and emission). To illustrate the influences of integral methods and increments in this study, a representative two-dimensional example derived from the EEMs of salt marsh water from excitation 240 to 300 nm with emission of 310 nm is displayed in Fig. 2. Rectangles are used in the Riemann summation, and the areas using 10-, 5-, and 1-nm increments are shown in Fig. 2a, b, and c, respectively. Trapezoids are formed between two adjacent points when using the composite trapezoidal rule, and the areas corresponding to three increments are shown in Fig. 2d, e, and f. Quadratic functions (Eq. [5]) are used to connect three adjacent points when using the composite Simpson's rule, and the areas corresponding to the three increments are shown Fig. 2g, h, and i. Although only the change in excitation increment was examined in this study, mathematically, the intervals of excitation and emission have the same effect on the numerical analysis and integration. These graphic illustrators demonstrate the difference in shapes of estimated areas under the three integral methods and show the importance of resolutions with three increments. Ideally, the smallest interval of excitation and emission increments should be used to obtain the most accurate data set for FRI.

Error Analysis

The nine samples we used in this study can represent different water sources and were able to show large peaks at different regions (Fig. 1). The FRI results of these samples confirmed that the composite Simpson's rule showed the best precision for EEM regional distribution with the same excitation increment of EEMs. The errors based on the composite trapezoidal rule and the composite Simpson's rule were significantly lower than Riemann summation (paired t test, both $n = 45$; $P < 0.001$). However, they were still high in Regions I and II, especially for natural waters (trapezoidal rule: 8.0–42.7%; Simpson's rule: 5.9–42.7%) (Supplemental Tables S3 and S4). Accumulated frequency of error based on our samples is estimated for reference (Fig. 3). The median error for 10-nm excitation using Riemann summation could be greater than 15%. However, in some cases, the error could be as large as 42% (Supplemental Tables S3 and S4). If the composite trapezoidal rule or the composite Simpson's rule is applied to the 10-nm excitation increment, the median error could be reduced to 5.1 and 4.5%, respectively. Therefore, 10-nm intervals with the composite Simpson's rule can be used only for rough estimation. In the original study by Chen et al. (2003), 5-nm excitation wavelength increments and the Riemann summation were suggested. With the original setting, most of the errors of normalized percentages could be controlled within 10%, and the median error is about 5%. The median error can be significantly improved to 1% by using the composite Simpson's rule. Although less accurate than using a 1-nm excitation increment, setting 5 nm as the excitation increment with the composite Simpson's rule can guarantee >95% normalized percentages having <5% error (Fig. 3). The measuring time and lamp cost of this setting are only about one fifth of the 1-nm excitation increment. Also, the computer runtime can be shortened in data collection when the 5-nm increment is compared with the 1-nm increment. For example, a sample takes more than 30 min for a 1-nm interval with a

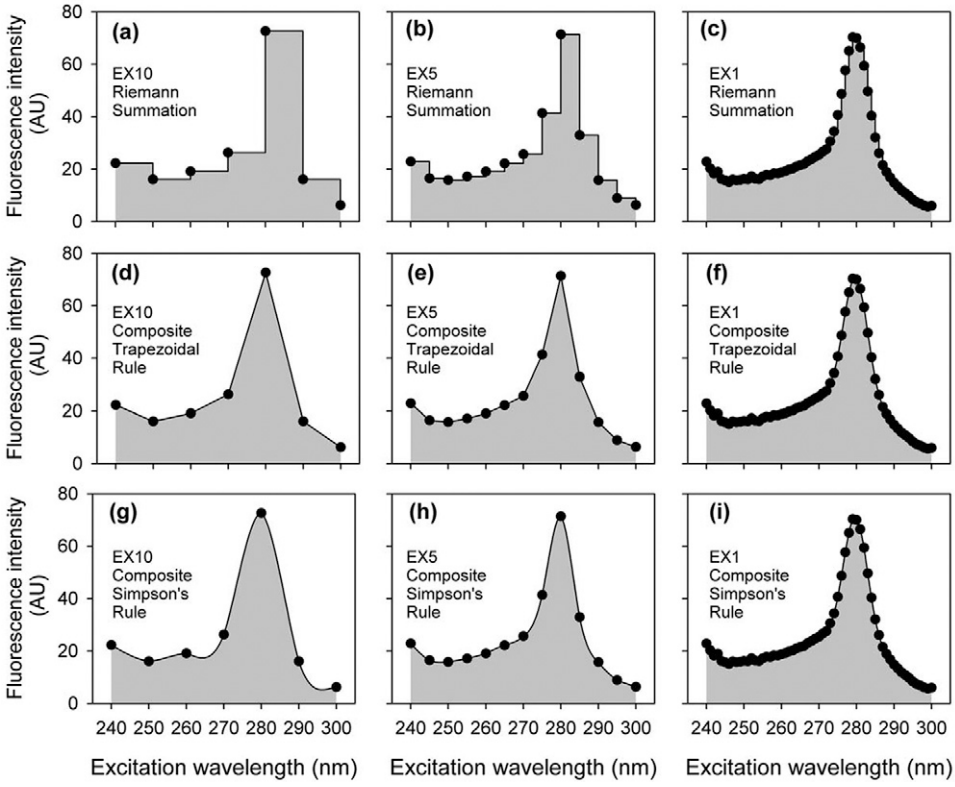

Fig. 2. Two-dimension demonstration shows the calculated areas using different numerical methods and excitation intervals.

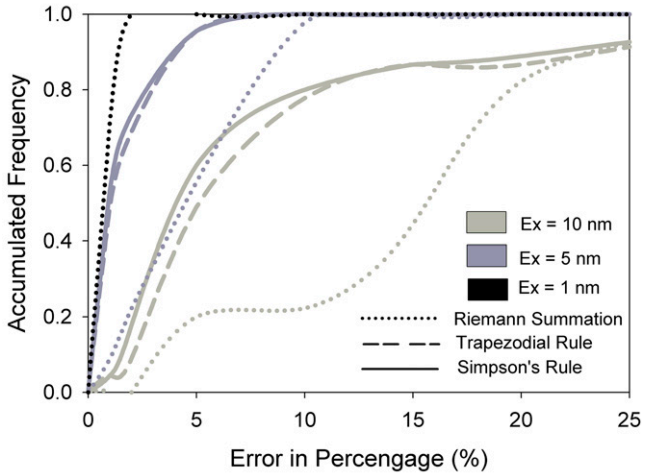

Fig. 3. Cumulative frequency distribution of errors in calculating fraction distribution using different numerical methods and excitation intervals.

medium scan speed but takes less than 10 min if a 5-nm interval is selected. In this case, using a 5-nm excitation increment is considered to be a cost-effective choice regarding the precision and measuring cost.

Recommendations

In this study, we tested the Riemann summation, the composite trapezoidal rule, and composite Simpson's rule for FRI analysis of fluorescence EEM with different excitation wavelength increments. Based on the results of this study, we recommend the following: (i) A 10-nm excitation increment is not appropriate for quantitative FRI analysis, and it can be applied for rough estimation only; (ii) Using the composite Simpson's rule to replace Riemann summation as integration method can enhance the precision of FRI analysis, regardless of the excitation increment used; (iii) With the composite Simpson's rule as integration method, using a 1-nm excitation increment is the most accurate for conducting the FRI analysis, whereas using a 5-nm excitation increment is a relatively cost-effective approach. If precision of 95 to 105% in FRI results is required using Riemann summation, the 1-nm excitation increment should be adopted. (iv) Results of this study show that the intervals of excitation and emission could affect the interpretation of EEMs. Although the mathematical logarithms of PARAFAC treating the data in fluorescence EEMs are completely different, we speculate that the interval effects on PARAFAC may also exist. (v) Instead of examining operationally defined regions in FRI, the trapezoidal rule or Simpson's rule can apply to components decomposed by PARAFAC components. Parallel factor analysis can decompose EEMs into components with similarly fluorescing moieties, with the loadings representing EX and EM spectra. The volume of each component can be quantified using the trapezoidal rule or Simpson's rule. A combination of PARAFAC and FRI may improve the accuracy and precision of dissolved organic matter characterization using fluorescence.

Acknowledgments

The authors thank Dr. William Conner at Baruch Institute of Clemson University for proofreading of earlier versions of the manuscript. Portions of this material were supported by the U.S. Geological Survey Climate and Land Use Change Research and Development Program, and by NIFA/USDA under project number SC-1700409. Technical Contribution no. 6105 of the Clemson University Experiment Station.

References

Burden, R.L., and J.D. Faires. 2001. Numerical analysis. 7th ed. Brooks/Cole Thomson Learning, Pacific Grove, CA.

Chen, W., P. Westerhoff, J.A. Leenheer, and K. Booksh. 2003. Fluorescence excitation- emission matrix regional integration to quantify spectra for dissolved organic matter. Environ. Sci. Technol. 37:5701–5710. doi:10.1021/es034354c

Chow, A.T., S. Gao, and R.A. Dahlgren. 2005. Physical and chemical fractionation of dissolved organic matter and trihalomethane precursors: A review. J. Water Supply Res. Technol. Aqua 54:475–507.

Coble, P.G. 1996. Characterization of marine and terrestrial DOM in seawater using excitation emission matrix spectroscopy. Mar. Chem. 51:325–346. doi:10.1016/0304-4203(95)00062-3

Cory, R.M., M.P. Miller, D.M. McKnight, J.J. Guerard, and P.L. Miller. 2010. Effect of instrument-specific response on the analysis of fulvic acid fluorescence spectra. Limnol. Oceanogr. Methods 8:67–78. doi:10.4319/lom.2010.8.0067

Fellman, J.B., E. Hood, and R.G.M. Spencer. 2010. Fluorescence spectroscopy opens new windows into dissolved organic matter dynamics in freshwater ecosystems: A review. Limnol. Oceanogr. 55:2452–2462. doi:10.4319/lo.2010.55.6.2452

He, X.S., B.D. Xi, Z.M. Wei, Y.H. Jiang, Y. Yang, D. An, J.L. Cao, and H.L. Liu. 2011. Fluorescence excitation-emission matrix spectroscopy with regional integration analysis for characterizing composition and transformation of dissolved organic matter in landfill leachates. J. Hazard. Mater. 190:293–299. doi:10.1016/j.jhazmat.2011.03.047

Henderson, R.K., A. Baker, K.R. Murphy, A. Hamblya, R.M. Stuetz, and S.J. Khan. 2009. Fluorescence as a potential monitoring tool for recycled water systems: A review. Water Res. 43:863–881. doi:10.1016/j.watres.2008.11.027

Hudson, N., A. Baker, and D. Reynolds. 2007. Fluorescence analysis of dissolved organic matter in natural, waste and polluted waters: A review. River Res. Appl. 23:631–649. doi:10.1002/rra.1005

Lawaetz, A.J., and C.A. Stedmon. 2009. Fluorescence intensity calibration using the Raman scatter peak of water. Appl. Spectrosc. 63:936–940. doi:10.1366/000370209788964548

Massicotte, P., and J.J. Frenette. 2011. Spatial connectivity in a large river system: Resolving the sources and fate of dissolved organic matter. Ecol. Appl. 21:2600–2617. doi:10.1890/10-1475.1

Miller, M.P., B.E. Simone, D.M. McKnight, R.M. Cory, M.W. Williams, and E.W. Boyer. 2010. Comment: New light on a dark subject. Aquat. Sci. 72:269–275. doi:10.1007/s00027-010-0130-2

Stedmon, C.A., S. Markager, and R. Bro. 2003. Tracing dissolved organic matter in aquatic environments using a new approach to fluorescence spectroscopy. Mar. Chem. 82:239–254. doi:10.1016/S0304-4203(03)00072-0

Wang, Z.W., Z.C. Wu, and S.J. Tang. 2009. Characterization of dissolved organic matter in a submerged membrane bioreactor by using three-dimensional excitation and emission matrix fluorescence spectroscopy. Water Res. 43:1533–1540. doi:10.1016/j.watres.2008.12.033

Wu, H.Y., Z.Y. Zhou, Y.X. Zhang, T. Chen, H.T. Wang, and W.J. Lu. 2012. Fluorescence-based rapid assessment of the biological stability of landfilled municipal solid waste. Bioresour. Technol. 110:174–183. doi:10.1016/j.biortech.2012.01.149